RSC Advances

PAPER

View Article Online
View Journal | View Issue

Cite this: *RSC Adv.*, 2018, **8**, 3958

Orthorhombic SnO_2 phase observed composite $(Sn_{1-x}Ce_x)O_2$ synthesized by sol–gel route†

M. H. Carvalho, *[a] E. C. Pereira[b] and A. J. A. de Oliveira *[a]

Received 23rd November 2017
Accepted 5th January 2018

DOI: 10.1039/c7ra12727h

rsc.li/rsc-advances

Semiconductor oxides are a class of materials used in many different applications, such as catalysis, solar cells and magnetic devices. In particular, composites with different semiconducting oxides follow synergetic effects with changes of electrical conductivity or magnetic properties. In this case, the synthesis conditions are very important for controlling their properties due to structural defects and non-stable phases at room temperature. In this paper, we analyzed the influence of the synthesis temperature and different concentrations of cerium in the formation of the orthorhombic SnO_2 phase. The structural and morphological characterization was performed using experimental techniques such as X-ray diffraction (XRD), allied with Rietveld refinement, field emission scanning electron microscopy (FE-SEM), transmission electron microscopy (TEM) and energy dispersive X-ray spectroscopy (EDS). The reflections in the XRD pattern and clear lattice fringes observed by HRTEM confirm the formation of the orthorhombic SnO_2 phase in the $(Sn_{1-x}Ce_x)O_2$ with $x = 0$, 0.05, 0.1 and 0.3 synthesized at 750 °C. The reducing atmosphere generated by the heat treatment process of the samples and the strain originated due to the difference of ionic radii between the tin and cerium ion can play a crucial role in the formation of the orthorhombic phase of SnO_2.

Introduction

Wide band gap semiconductor oxides, such as tin dioxide (SnO_2), are the subject of intensive research due to the their applications in different areas, such as gas sensors,[1,2] solar cells,[3] catalysts[4] and optoelectronic devices.[5] This oxide can be synthesized in three different crystalline phases: tetragonal, orthorhombic and cubic. The most thermodynamically stable phase, at room temperature, is cassiterite, a rutile crystalline structure with tetragonal symmetry (space group $P4_2/mnm$). Orthorhombic and cubic phases are metastable and can be obtained using synthesis under high pressure and temperature, or from a phase transition of the rutile structure at high pressure.[6,7] From a different point of view, the orthorhombic SnO_2 phase (O-SnO_2) exhibits distinct physical and chemical properties compared to the stable phase (tetragonal), motivating the development of synthesis routes to obtain it. With this purpose, the optimization of the O-SnO_2 synthesis under atmospheric pressure allows exploring the new magnetic and optical properties, thus, opening new perspectives for different applications.

The formation of the orthorhombic phase is directly related to the synthesis method used, as well as to other experimental conditions, such as pressure, and temperature. Although originally this phase was found only in experiments carried out at high pressure and temperature, new synthesis strategies have been proposed to prepare O-SnO_2 under atmospheric pressure. In this sense, different physical and chemical routes, such as pulsed laser deposition (PLD)[8,9] oxidizing epitaxial tin monoxide films,[10] metalorganic chemical vapor deposition (MOCVD)[11] and co-precipitation methods[12] were used to synthesize this phase. For example, Chen *et al.* prepared pure O-SnO_2 thin films at a pressure of 3×10^{-2} Pa and substrate temperature of 320 °C using pulsed laser deposition (PLD).[8] Lamelas *et al.* investigated the formation of nanoparticles with orthorhombic phase produced by the oxidation of mechanically milled tin monoxide powders, followed by a heating to 575 °C.[13] Using a different approach, Zhang *et al.*, proposed to dope the SnO_2 with Mn to obtain the orthorhombic phase. The authors reported a mixture of O-SnO_2 and T-SnO_2 for samples processed at ambient pressure doped with 5 mol% of Mn.[12] Using a similar strategy, we investigated the doping process of SnO_2 with a rare earth metal (RT). Among the RT, we chose cerium doping, since it has two oxidation states and ionic radius with the coordination number equal to 6, Ce^{3+} (1.01 Å) and Ce^{4+} (0.87 Å), respectively, much larger than the Sn^{4+} (0.69 Å), with the same coordinate number.[14] This could induce stress in the SnO_2 lattice, possibly leading to the formation of the orthorhombic phase.

[a]*Physics Department, Federal University of São Carlos, UFSCar, P. O. Box 676, 13565-905, São Carlos, SP, Brazil. E-mail: adilson@df.ufscar.br; helenacarvalho@df.ufscar.br*

[b]*Chemistry Department, LIEC, Federal University of São Carlos, UFSCar, P. O. Box 676, 13565-905, São Carlos, SP, Brazil*

† Electronic supplementary information (ESI) available. See DOI: 10.1039/c7ra12727h

From a different point of view, sol–gel routes, such as, the Pechini method,[15] have not been used to prepare this oxide phase. Then, considering the importance of orthorhombic SnO_2 and the lack of papers using sol-routes to synthesize it, the aim of this work is the synthesis and structural characterization orthorhombic phase of SnO_2 in the nanoparticle system $(Sn_{1-x}Ce_x)O_2$, with $x = 0$, 0.05, 0.1, 0.3, 0.7 and 1.0 using the Pechini method.

Experiment details

Nanoparticles of $(Sn_{1-x}Ce_x)O_2$ were produced using the Pechini method[15] with different Ce molar concentrations ($x = 0$, 0.05, 0.1, 0.3, 0.7, 1) and synthesis temperatures. Initially, in an 0.5 L of an aqueous solution of 0.25 mol L^{-1} citric acid (P A Synth), 28.20 g of tin chloride dihydrate (Sigma-Aldrich) was added. The final solution pH was controlled using 1 M/L ammonia solution (Synth) added drop wise until its value is 3. Then, a white powder of tin citrate was obtained.[16] The precipitate was washed with 0.7 L of distilled water and dried in the oven at 70 °C for 24 h, resulting in the tin citrate monohydrate ($C_6H_4O_7Sn_2 \cdot H_2O$).[16] Next, the precursor solution were prepared by dissolving 2×10^{-3} mol tin citrate monohydrate ($C_6H_4O_7Sn_2 \cdot H_2O$) in 4.46 mL ethylene glycol, EG, (Sigma-Aldrich) under stirring at 70 °C, leading to a solution of 0.45 mol L^{-1}. It was necessary to add 80 μL of concentrated nitric acid to completely dissolve the salt. Separately, 2×10^{-3} mol ammonium cerium(IV) nitrate $(NH_4)_2Ce(NO_3)_6$ (Vetec) was dissolved in 4.46 mL of EG, under stirring at 70 °C. Afterward, separately, 2×10^{-2} mol citric acid (CA – P A Synth) was added to these solution, keeping it at constant temperature and stirring. All samples were prepared with the molar ratio of 1 : 10 : 40 of total metal salt : citric acid : ethylene glycol, respectively. Then, the proper molar amount of cerium salt solution was added to the Sn salt solution in the following oxide molar composition: 0, 0.05, 0.10, 0.30, 0.70, 1.00. Then, the solutions were polymerized at 110 °C for 1 h and immediately thermal treated using two steps: (i) at 300 °C for 2 hours using a heating rate of 10 °C min^{-1}, to inhibit aggregate formation and, (ii) different final temperatures (500, 580, 650 or 750 °C) for 2 hours to obtain the doped oxides. The second thermal treatment used also 10 °C min^{-1} as heating rate. The color of the pure SnO_2 is white powder, and, for those samples doped with cerium, their color become yellow.

The crystalline structures of the samples were investigated by X-ray diffraction (XRD) using a Rigaku powder diffractometer (Model D/Max-2500PC) with CuK_α radiation with Bragg–Brentano geometry mode θ–2θ in the range 20–100° at a scan speed of 0.5° min^{-1}, with a step of 0.02°. Rietveld refinements[17] were performed using the free GSAS-EXPGUI software.[18,19] The quality of the fitting procedure can be followed using the goodness of fit (S parameter). It is described in the literature if S is close to 1 indicate an excellent fitting process.[20]

The morphology and size of the nanoparticles were examined by Field Emission Scanning Electron Microscopy (FE-SEM) using Supra 35-VP Carl Zeiss, operated at 15 kV and by high-resolution Transmission Electron Microscopy (HRTEM) technique, using an FEI microscope (model Tecnai G2 F20, FEI), 300 kV. The chemical analyses of the samples were performed by EDS using a Thermo-Noran EDS.

Results and discussion

Fig. 1 shows X-ray diffraction patterns measured at room temperature for SnO_2 samples, synthesized at 500 (a), 580 (b), 650 (c) and 750 °C (d). The orange and violet vertical bars correspond to the indexation to the Inorganic Crystal Structure Database, (ICSD no. 39173 and 157450) for the tetragonal and orthorhombic phase SnO_2, respectively.

The XRD patterns shown in Fig. 1a to c are consistent with the tetragonal SnO_2 phase (space group: $P4_2/mnm$) with lattice parameters, $a = b = 4.7358$ Å and $c = 3.1851$ Å.[21] Within the limit of resolution in XRD the detection of additional reflections were observed, which excludes the presence of a crystalline secondary phase. In Fig. 1d, samples prepared at 750 °C, in addition to the clear presence of SnO_2 tetragonal (marked circles), a second phase, O-SnO_2 peaks was identified. In fact, Bragg peaks (11l) and (02l) (see squares labels in Fig. 1d) correspond to the orthorhombic SnO_2 (space group: $Pbcn$) with lattice parameters, $a = 4.707$ Å, $b = 5.710$ Å and $c = 5.246$ Å.[22] Moreover, the weak diffraction peak at $2\theta = 30.6°$ and 44.9°, labeled by an asterisk in Fig. 1d, can be indexed as the plane (200) and (211) of the metallic tin phase (Sn), in agreement with that reported in the literature[23] (ICSD no. 40038).

The XRD patterns were analyzed using Rietveld refinement.[17] A pseudo-Voigt function of Thompson-Cox-Hasting modified by Young and Desai (pV-TCHZ) as the profile function[24] used in the fitting process. The full width at half maximum (FWHM) obtained from this procedure was used to estimate the crystallite size $\langle D_{X\text{-ray}} \rangle$ and is presented in Table 1. In addition, lattice

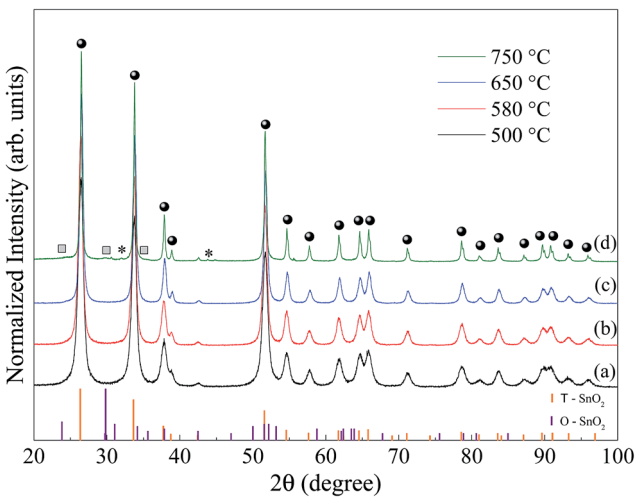

Fig. 1 X-ray diffraction patterns for the SnO_2 calcined, (a) 500, (b) 580, (c) 650 and (d) 750 °C for 2 hours. The circles and squares denote the tetragonal and orthorhombic SnO_2 peaks, respectively; the asterisk denotes the peaks of metallic Sn; the orange and violet bars, respectively, correspond to the indexation of the diffraction peaks for SnO_2 tetragonal (ICSD 39173) and orthorhombic (ICSD 157450).

Table 1 Lattice parameters, unit cell volume, crystallite size, lattice strain and goodness of the fit procedure, obtained from the Rietveld refinement data for SnO_2 calcined at 500, 580, 650 and 750 °C. With, (T) tetragonal phase, (O) orthorhombic phase and (M) metallic phase

	Lattice parameter (Å)						
Temp (°C)/phase	a (Å)	b (Å)	c (Å)	Cell volume V (Å^3)	$\langle D_{X\text{-ray}} \rangle$ (nm)	Strain (%)	S
500/T	4.735	4.735	3.185	71.40	19.3	0.3411	1.34
580/T	4.735	4.735	3.185	71.41	29.8	0.5127	1.48
650/T	4.742	4.742	3.188	71.67	29.9	0.6261	1.52
750/T	4.740	4.740	3.188	71.62	50.3	0.1260	
750/O	4.727	5.650	5.271	140.10	4.8	3.6819	1.82
750/M	5.828	5.828	3.178	107.90	40.4	1.0480	

parameters, unit cell volume, lattice strain and goodness of fit, (S), obtained by the Rietveld refinement are also listed in Table 1.

The goodness of fit indicator S shows the good quality of structural refinement data. A change was observed in the lattice parameters and consequently in the volume of the unit cell as a function of the increase in the synthesis temperature.

As shown in Fig. 1 there is a narrowing in the FWHM of the Bragg peak with increasing synthesis temperature. Part of this narrowing is due to the increase in the crystallite size, as calculated by Rietveld refinement (Table 1), which is in good agreement with the literature.[25] For the sample calcined at 750 °C, Table 1 shows that the size of the crystallite of the majority phase, tetragonal SnO_2, is much larger compared to the size of the crystallite of the orthorhombic SnO_2. In contrast, we obtained the highest strain value for the orthorhombic SnO_2 and a lower value for tetragonal SnO_2.

Fig. 2a shows SEM image for the SnO_2 sample calcined at 750 °C. In the inset the particle size histogram was obtained from several SEM images fitted by a log-normal distribution. It clearly observed that pure SnO_2 particles are larger (48.0 ± 0.2) and have non-uniform sizes compared to the pure sample calcined at 650 °C (29.4 ± 0.3). These data are shown in Fig. SI.1 (ESI†). High-resolution TEM images (Fig. 2b and c) also show that this sample is highly crystalline, which is clearly observed from the Fourier transform (Fig. 2d) of the image. It is possible to observe two sets of planes with lattice spacing of 3.64 Å and 2.98 Å, respectively, corresponding to planes (110) and (111) of the orthorhombic of SnO_2 phase. It was also possible to observe a plane at 3.34 Å, which corresponds to the plane (110) of the tetragonal SnO_2 phase (Fig. 2c). The TEM results confirm that both phases of tetragonal SnO_2 and orthorhombic coexist in the sample even in the case of non-doped material, $x = 0$, synthesized at 750 °C, which is consistent with XRD data (see Fig. 1).

Recent studies developed by Zhang *et al.*[12] reported the formation of the orthorhombic phase in SnO_2 at atmospheric pressure, for samples doped with 5 mol% of Mn, synthesized by co-precipitation. The authors proposed the formation of this phase with distortion of the lattice generated by the doping process of tetragonal SnO_2.[12] Based on this paper, we decided to study the solubility limit of cerium in SnO_2. It is known that the Ce^{4+} ion has an ionic radius equal to 0.87 Å with coordination number equal to 6 and Sn^{4+} is smaller (ionic radius = 0.69 Å), with the same coordination number.[14] Therefore, the doping of SnO_2 using Ce could induce distortions in the lattice, increasing the concentration of the orthorhombic SnO_2 phase.

Fig. 3a shows TEM images for the sample $x = 0.3$ calcined at 750 °C. A spherical morphology and a reduction in particle size are observed, compared to the undoped sample (Fig. 2a). Fig. 3b shows the HRTEM image which confirms both SnO_2 phases, with the d-spacing at 3.34 Å and 2.98 Å corresponding to the tetragonal (110) and orthorhombic (111) planes, respectively. We also observed the d-spacing at 3.12 Å, which corresponds to the plane (111), confirming the segregation of the CeO_2 cubic phase. The energy-dispersion X-ray spectroscopy (EDS)

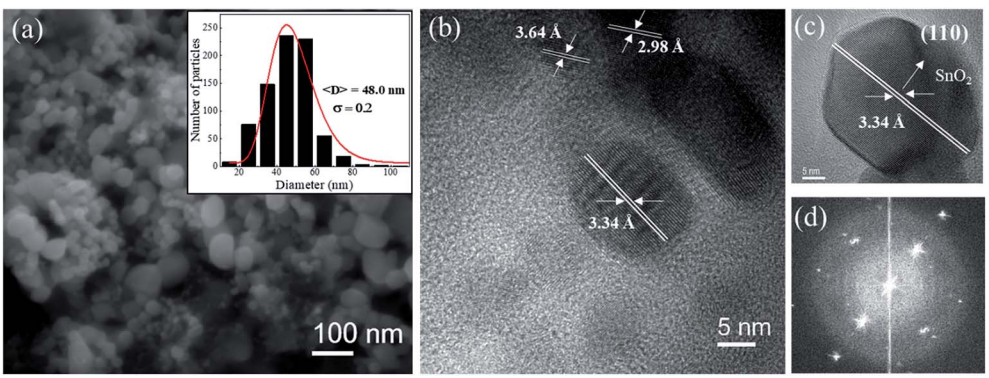

Fig. 2 (a). FE-SEM image of the sample SnO_2 calcined at 750 °C. (b) HRTEM image of a set of nanoparticles. (c) HRTEM image of an individual SnO_2 nanoparticle indicating the interplanar distances characteristic of tetragonal tin dioxide and the corresponding Fourier transform in (d). The insert: particle size histogram fitted with a log-normal size distribution.

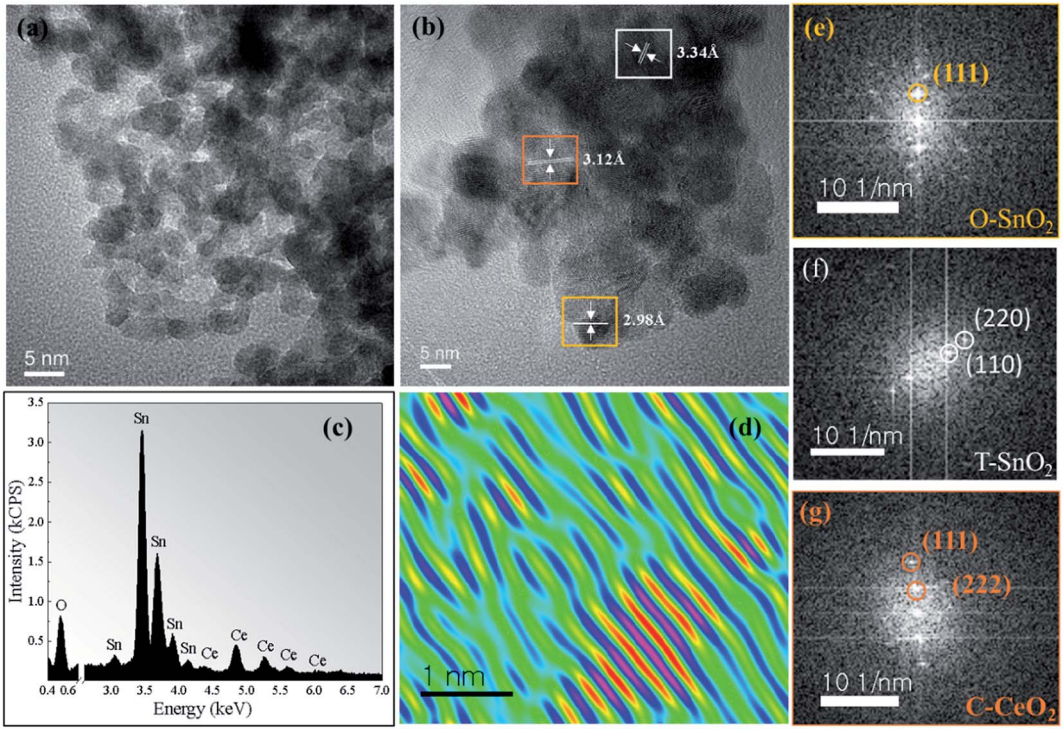

Fig. 3 (a) TEM image of the sample $x = 0.3$ calcined at 750 °C. (b) HRTEM image (c) EDS spectrum of the sample. (d) Reconstructed HRTEM image of a CeO_2 particle, which shows the lattice mismatch between CeO_2 plans. (e–g) FFT pattern referring to the orthorhombic (O-SnO_2), tetragonal (T-SnO_2) phase and the cubic (C-CeO_2) phase.

characterization (Fig. 3c) confirms that the synthesized sample is composed only of Sn, Ce, and O and the quantitative analysis of both Sn and Ce molar ratios of the experimentally and nominally obtained composition is in good agreement, which is presented in Table SI.2 (ESI†). Fig. 3d shows the reconstructed HRTEM image of one region corresponding to CeO_2 particle. It is clearly observed that the sample has structural defects, observed in the Figure by the lack of linear behavior of the crystalline planes. It is possible this occurs due to the distortions in the atomic planes of the CeO_2 phase. In the Fig. 3e–g, respectively, the FFT pattern obtained from each region of Fig. 3b is shown, *i.e.*, orthorhombic and tetragonal SnO_2 phase and the cubic CeO_2 phase.

The XRD patterns for the samples $(Sn_{1-x}Ce_x)O_2$ changing the molar concentration of Ce ($x = 0$, 0.05, 0.1, 0.3, 0.7, 1) calcined at 750 °C for 2 hours are shown in Fig. 4. We also show the difference (blue line) between the experimental and calculated patterns, which were evaluated by the Rietveld method. All patterns shown in Fig. 4 indicate that both structures, tetragonal and orthorhombic of SnO_2 coexist within the samples in the range from 0 to $x = 0.3$. No diffraction peak associated to the formation of cerium oxide (CeO_2) was detected up to the concentration $x = 0.1$. However, by increasing the concentration to higher values, $x = 0.3$, 0.7 and 1, the Bragg peaks of CeO_2 fluorite structure can be observed space group: $Fm\bar{3}m$ and lattice parameter, $a = b = c = 5.4124$ Å (ICSD no. 72155).

The structural parameters calculated by the Rietveld refinement are listed in Table 2, which show a molar percentage for each phase, lattice parameters, unit cell volume, crystallite size, lattice strain and goodness of fit values, which is an indicator that the refinement quality is suitable. Table 2 shows that while the unit cell volume of the tetragonal SnO_2 did not present significant changes as the Ce concentration increases 10 mol%, the orthorhombic of SnO_2 phase exhibits an expansion in the structure, *i.e.*, there is an increase in the volume of the unit cell,

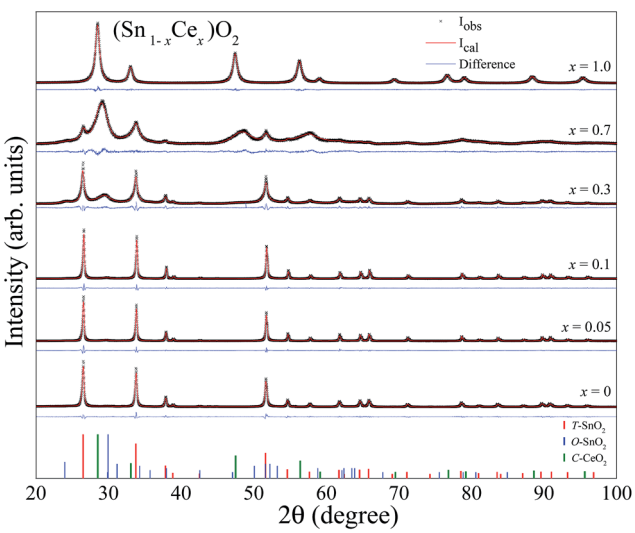

Fig. 4 X-ray diffraction patterns for the $(Sn_{1-x}Ce_x)O_2$ ($x = 0$, 0.05, 0.1, 0.3, 0.7, 1) nanoparticles synthesized at 750 °C. The solid lines are the fittings using the Rietveld method (red lines) and difference between the experimental and calculated patterns (blue lines).

Table 2 List of parameters obtained from the Rietveld refinement of the XRD patterns for the $(Sn_{1-x}Ce_x)O_2$ (x = 0, 0.05, 0.1, 0.3, 0.7, 1) nanoparticles synthesized at 750 °C. Phase, molar percentage for each phase, lattice parameters, unit cell volume, crystallite size, lattice strain and goodness of the fit procedure

			Lattice parameter (Å)						
$(Sn_{1-x}Ce_x)O_2$	Phases	(% molar)	a (Å)	b (Å)	c (Å)	Cell volume V (Å^3)	$\langle D_{X\text{-ray}}\rangle$ (nm)	Strain (%)	S
$x = 0$	T-SnO_2	87.58	4.740	4.740	3.188	71.62	50.3	0.1260	1.82
	O-SnO_2	11.27	4.727	5.650	5.271	140.10	4.8	3.6819	
	M-Sn	1.15	5.828	5.828	3.178	107.90	40.4	1.0480	
$x = 0.05$	T-SnO_2	88.97	4.740	4.740	3.188	71.62	74.3	0.1087	1.90
	O-SnO_2	10.46	4.768	5.633	5.304	142.40	12.6	3.6086	
	M-Sn	0.57	5.827	5.827	3.183	108.13	9.7	0.9295	
$x = 0.1$	T-SnO_2	89.65	4.740	4.740	3.188	71.62	74.9	0.1087	1.78
	O-SnO_2	9.44	4.701	5.719	5.305	142.60	12.2	4.0458	
	M-Sn	0.91	5.828	5.828	3.171	107.70	27.6	1.0337	
$x = 0.3$	T-SnO_2	50.87	4.743	4.743	3.187	71.70	25.0	0.1125	1.76
	O-SnO_2	40.90	4.798	5.658	5.282	143.40	6.5	3.3376	
	CeO_2	8.23	5.323	5.323	5.323	150.70	3.6	1.1425	
$x = 0.7$	T-SnO_2	26.43	4.748	4.748	3.196	72.05	13.7	1.4380	1.33
	CeO_2	73.57	5.325	5.325	5.325	151.06	18.8	8.3392	
$x = 1$	CeO_2	100	5.416	5.416	5.416	158.89	14.1	0.0829	1.17

suggesting the formation of a substitutional solid solution. Since, Ce^{4+} ions have a larger ionic radius than Sn^{4+}, with the same coordination number, its incorporation into the orthorhombic SnO_2 structure justify the increase of the volume of the unit cell. However, the solubility of Ce ions in SnO_2 without phase segregation is limited to 10 mol%. Above this concentration, the segregation of cerium oxide phase can be observed. Table 2 shows that the crystallite size of T-SnO_2 is much larger than that of O-SnO_2 and presents lower strain values. This probably occurs due to the decrease in internal stresses when crystallite size increases. Another important characteristic due to the incorporation of cerium in SnO_2 is the disorder in the crystalline structure created by the stacking faults in the crystal due to the difference of ionic radius, resulting in increased strain.

Fig. 5 shows the summarization of these results plotting the molar concentration obtained by the Rietveld refinement for each oxide as a function of the nominal Ce concentration. The results show that the introduction of different Ce concentrations produces different conditions to stabilize the orthorhombic phase of SnO_2. This Figure corroborates the data presented in Fig. 4, in which the amount of O-SnO_2 phase increases as the Ce nominal concentration increases to 30 mol%. The maximum amount of O-SnO_2 obtained is 41% for the sample synthesized at 750 °C with 30 mol% of Ce dopant.

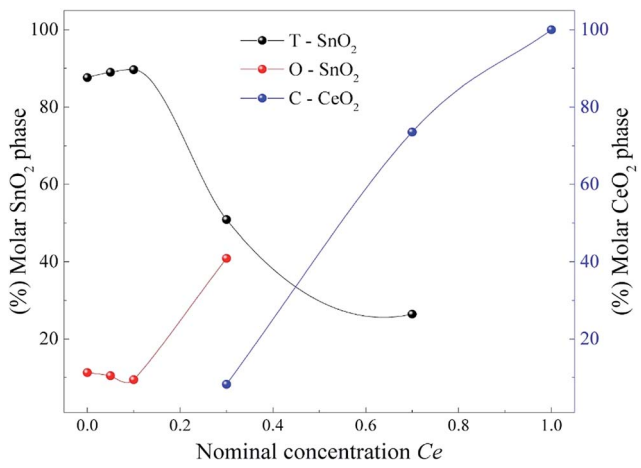

Fig. 5 Molar concentration obtained by the Rietveld refinement for each oxide as a function of the nominal Ce concentration.

It is well established in the literature that the orthorhombic SnO_2 phase was originally observed only in experiments with high pressures and temperatures.[8,9] However, recently Zhang *et al.* using the chemical co-precipitation method, reported the formation of the orthorhombic phase of SnO_2 at atmospheric pressure, when the samples were doped with 5 mol% of Mn.[12] Our results show that the orthorhombic phase already appears in the pure sample, although with a small molar fraction, reaching a molar fraction of approximately 41% when we increase the concentration of Ce to $x = 0.3$ (see Fig. 5).

The Pechini method proved to be an effective alternative for the synthesis of orthorhombic SnO_2, possibly due to the number of defects generated in the thermal treatment process. However, the process of incorporating Ce in the SnO_2 phase led to an increase in the concentration of the orthorhombic phase, possibly due to the ionic radius difference of Ce^{4+} (0.87 Å) and Sn^{4+} (0.69 Å) leading to the disorder of the crystal structure created by stacking faults in the crystal.

Conclusions

In this work, we have successfully obtained nanoparticles of $(Sn_{1-x}Ce_x)O_2$ using the Pechini method. The reflections on the XRD pattern and clear lattice fringes observed in the HRTEM images confirm the formation of the orthorhombic of SnO_2 phase with x = 0, 0.05, 0.1 and 0.3, synthesized at 750 °C. Through the Rietveld refinement analyzes it can be observed

that the sample with 0.3 moles of cerium reaches a significant molar fraction of the orthorhombic phase, approximately 41%. The reducing atmosphere generated by the heat treatment of the samples and the strain originated due to the difference of ionic rays between the tin and cerium ion can play a crucial role in the formation of orthorhombic phase SnO_2. The synthesis method used proved to be a promising alternative route for the preparation of orthorhombic SnO_2.

Conflicts of interest

There are no conflicts to declare.

Acknowledgements

This work was supported by the FAPESP (2013/07296-2 and 2017/24995-2), CAPES and CNPq Brazilian agencies.

References

1 L. Renard, O. Babot, H. Saadaoui, H. Fuess, J. Brötz, A. Gurlo, E. Arveux, A. Klein and T. Toupance, *Nanoscale*, 2012, **4**, 6806–6813.
2 J. Arbiol, E. Comini, G. Faglia, G. Sberveglieri and J. R. Morante, *J. Cryst. Growth*, 2008, **310**, 253–260.
3 C. C. Sno, S. Cells, A. Hossain, J. R. Jennings, Z. Y. Koh and Q. Wang, *ACS Nano*, 2011, **5**, 3172–3181.
4 A. Dodd, A. McKinley, M. Saunders and T. Tsuzuki, *Nanotechnology*, 2006, **17**, 692–698.
5 H.-S. Woo, I.-S. Hwang, C. W. Na, S.-J. Kim, J.-K. Choi, J.-S. Lee, J. Choi, G.-T. Kim and J.-H. Lee, *Mater. Lett.*, 2012, **68**, 60–63.
6 J. Haines and J. M. Le, *Phys. Rev. B: Condens. Matter Mater. Phys.*, 1997, **55**, 144–154.
7 L. G. Liu, *Science*, 1978, **199**, 422–425.
8 Z. Chen, J. K. L. Lai and C.-H. Shek, *Appl. Phys. Lett.*, 2006, **89**, 231902.
9 F. J. Lamelas and S. A. Reid, *Phys. Rev. B: Condens. Matter Mater. Phys.*, 1999, **60**, 9347–9352.
10 A. Prodan, N. Vene, F. Sevgek and M. Hudomalj, *Thin Solid Films*, 1987, **147**, 313–319.
11 L. Kong, J. Ma, Z. Zhu, C. Luan, X. Yu and Q. Yu, *Mater. Lett.*, 2010, **64**, 1350–1353.
12 Q. Zhang, P. Liu, C. Miao, Z. Chen, C. M. Lawrence Wu and C.-H. Shek, *RSC Adv.*, 2015, **5**, 39285–39290.
13 F. J. Lamelas, *J. Appl. Phys.*, 2004, **96**, 6195.
14 R. D. Shannon, *Acta Crystallogr., Sect. A: Cryst. Phys., Diffr., Theor. Gen. Crystallogr.*, 1976, **32**, 751–767.
15 M. P. Pechini, Method of preparing lead and alkaline earth titanates and niobates and coating method using the same to form a capacitor, US3330697 A, Patent, 1967.
16 M. M. Besso, Tin salts of citric acid and method of preparation, US3213120, Patent, 1965.
17 R. A. Young, *The Rietveld Method. I.U.C*, Oxford University Press Inc., New York, 1995.
18 A. C. Larson and R. B. Von Dreele, *Los Alamos Natl. Lab. Rep.*, 2004, pp. 86–748.
19 B. H. Toby, *J. Appl. Crystallogr.*, 2001, **34**, 210–213.
20 L. B. McCusker, R. B. Von Dreele, D. E. Cox, D. Louër and P. Scardi, *J. Appl. Crystallogr.*, 1999, **32**, 36–50.
21 H. Seki, N. Ishizawa, N. Mizutani and M. Kato, *Powder Diffr.*, 1989, **4**, p156–p160.
22 L. Gracia, A. Beltrán and J. Andrés, *J. Phys. Chem. B*, 2007, **111**, 6479–6485.
23 J. A. Lee and G. V. Raynor, *Proc. Phys. Soc., London, Sect. B*, 1954, **67**, p737–p747.
24 R. Young and P. Desai, *Arch. Nauki Mater.*, 1989, **10**, 71–90.
25 A. Maciel, P. Lisboa-Filho, E. Leite, C. Paiva-Santos, W. Schreiner, Y. Maniette and E. Longo, *J. Eur. Ceram. Soc.*, 2003, **23**, 707–713.